Journal of Magnetism and Magnetic Materials 527 (2021) 167756

Contents lists available at ScienceDirect

Journal of Magnetism and Magnetic Materials

journal homepage: www.elsevier.com/locate/jmmm

Research articles

A performance improved ACFM-TMR detection system with tradeoff denoising algorithm

Lingsi Sun [a,b,c], Shuxiang Zhao [a,b,c], Ying Shen [a,b,c], Jiazeng Wang [a,b,c], Junqi Gao [a,b,c,*]

[a] Acoustic Science and Technology Laboratory, Harbin Engineering University, Harbin 150001, China
[b] Key Laboratory of Marine Information Acquisition and Security (Harbin Engineering University), Ministry of Industry and Information Technology, Harbin 150001, China
[c] College of Underwater Acoustic Engineering, Harbin Engineering University, Harbin 150001, China

ARTICLE INFO

Keywords:
ACFM detection system
Detection performance
TMR sensor
Wavelet
Tradeoff (*TO*) method
Wavelet selection

ABSTRACT

This paper presents a novel alternating current field measurement (ACFM) system, which is realized by tunneling magnetoresistive (TMR) sensors and a tradeoff (*TO*) wavelet denoising algorithm. The TMR sensor is characterized with a high sensitivity of 30 mV/V/Oe and a self-noise of less than 9pT/$\sqrt{\text{Hz}}$ at driving frequency $f = 3$ kHz. *TO* algorithm is proposed to select the optimum combination of mother wavelet family and decomposition level. The combinations of wavelet *Db5* with decomposition level 8 and *Sym7* with decomposition level 8 are determined as the most suitable ones for x- and z-axis signal denoising respectively, which have been demonstrated to be better than the traditional low-pass filtering method. Finally, the efficiency of the proposed system is proved by an experiment under more pressing test conditions, for example, with increased lift-off distance of 10 mm. In particular, it leads to increased *SNR* (signal-to-noise ratio) by 25.5 dB and 16.5 dB for x- and z-axis ACFM signal, respectively.

1. Introduction

As one of the most widely-used nondestructive testing (NDT) techniques, alternating current field measurement (ACFM) aims to detect and measure defects in the essential parts of industrial devices [1]. The technique adopts an ACFM inductor to produce a uniform electromagnetic field on the surface of a workpiece, where the magnetic field emanated from the load current can be detected by sensitive magnetic sensors. ACFM is developed with an inverse algorithm to predict crack damage level from measured sensor output signals, and many researchers have successfully applied this method in the cracks detection and characterization for safety–critical structures [2,3]. Li *et al.* studied the optimal lift-off values for the U-shaped ACFM probe by simulations and experiments which is helpful to size the cracks precisely [4]. L. Nicholson *et al.* developed a model to describe the relationship between the rolling contact fatigue (RCF) cracks and the signal collected by ACFM sensor [5]. Ali Akbari-Khezri1 *et al.* proposed a method for reconstructing the depth profile of a surface-breaking crack in a cylindrical metal using the output signal of an ACFM probe [6]. Noroozi *et al.* proposed a fuzzy learning approach for identification of arbitrary crack [7]. Rowshandel *et al.* reported a method to size the subsurface section of multiple cracks by artificial neural network (ANN) [8]. Zhao *et al.* presented a single-axis ACFM detection system to evaluate the crack length and depth [9].

The ongoing development of magnetoresistance (MR) elements offers updated technology in ACFM detection. At present, the most prominent magnetic sensors used for NDT applications include Hall effect [10], anisotropic magnetoresistors (AMRs) [11], giant magnetoresistors (GMRs) [12,13], and Tunneling magnetoresistive TMRs [14–18]. The largest MR ratios reached by TMR effect, which directly governs the sensitivity of the sensors, were reported with 500% at room temperature and 800% at 5 K respectively [19–21]. It is at least 10 × larger than that of AMR and GMR effects. However, the ultimate performance-limiting factor of TMR sensors for NDT application is determined not only by the sensitive response to an incident magnetic field, but also by a sensor's intrinsic noise in absence of an incident field.

In ACFM applications, it is of primary importance to extract the desired characteristic signal under the condition of presence of noise [22,23]. However, it is inevitably contaminated by noise nuisance which can smear out the sharp variations induced by the target cracks. Thus, reliable denoising is a basic and principal step in ACFM signal processing, which helps to overcome the restriction in real application. Wavelet

* Corresponding author at: College of Underwater Acoustic Engineering, Harbin Engineering University, Harbin 150001, China.
E-mail address: gaojunqi@hrbeu.edu.cn (J. Gao).

https://doi.org/10.1016/j.jmmm.2021.167756
Received 23 November 2020; Received in revised form 23 November 2020; Accepted 9 January 2021
Available online 22 January 2021

transform has been largely used in signal denoising and data compressing fields, which relies on the strong correlation between the signal and wavelet [24,25]. It is well known that the signal mostly corresponds to the large amplitude of the wavelet coefficients, whereas the noise always maps with the ones having small amplitude values. Comparing with available time–frequency analysis methods such as short-time fourier transform (STFT), wavelet transform has been demonstrated to be desirable for signal denoising due to its enhanced detectability and abundance of mother wavelet families [26,27]. However, this advantage leads to a question what is the most appropriate mother wavelet family for a particular signal? Indeed, there has been no experimental report so far on the dependence of wavelet base choosing on denoising effect for ACFM.

Here, we present the realization of a performance improved ACFM-TMR detection system with a *TO* denoising algorithm. The TMR sensor is characterized with a high sensitivity around 30 mV/V/Oe in a linear range of ± 10 Oe and a self-noise of only 10pT/$\sqrt{\text{Hz}}$ at frequency higher than 3 kHz. *TO* is a multi-criteria evaluation system using four standard evaluating criteria which are *CC* (correlation coefficient), *SNR* (signal to noise ratio), *MSE* (mean square error) and *F* (flatness) [28]. Recent studies have shown the employment of some of the evaluating metrics to choose a desired wavelet base for signal denoising [28,29]. But such denoising method has limitations in real applications, as its insufficient consideration for the whole assessment factors resulting in a biased evaluation. The *TO* method is able to provide a comprehensive perspective to evaluate the denoising quality under the combinations of different wavelet bases and decomposition levels (*DLs*). The specific combination with the largest *TO* value is determined to have the best denoising quality. The optimal wavelet method shows better performance than traditional used LPF (low-pass filter). The enhanced detectability of this system is demonstrated by tough experimental conditions with weak excitation signal.

2. ACFM detection setup

2.1. TMR sensor

Considering the high sensitivity and low noise of TMR technology, TMR sensing elements from MultiDimension Technology (China) are used. The magnetic field sensitivity is firstly characterized as a function of a magnetic field (*H*) for the TMR sensing elements, which are excited by a voltage bias of $V_{\text{bias}} = 1$ V along their sensing axis using electromagnets. As shown in Fig. 1 (a), the output voltage transfer curves of x- and z-axis TMR sensing elements exhibit similar trends with *H*, and the value of sensitivity is determined by the slope of the transfer curve. In linear range of $H = \pm 10$ Oe, the sensitivity of 30.2 (x-axis) and 27.8 (z-axis) mV/V/Oe are observed for the two sensing elements.

To build a magnetic sensor device, we properly customize a conditioning circuit for the TMR sensing elements to amplify the signal and filter out the unexpected low-frequency noise. Due to the typical excitation frequency bandwidth, the circuit is designed to work at a frequency bandwidth of $f \geq 1.6$ kHz as shown in Fig. 1 (b). Furthermore, with the help of the instrumentation amplifier, the circuit is developed with a gain transfer function of 100 times (40 dB) over the frequency bandwidth of 1.6 to 10 kHz. The equivalent magnetic noise for the TMR sensor is then measured in the frequency range of $0.1 < f < 10^4$ Hz inside a zero-Gauss magnetically shielding chamber. The sensor analogue output signal is then sent to a dynamic signal analyzer (SR785, Stanford Research Systems, USA) for analysis. The sensor self-noise is acquired and recorded as a voltage output spectral density in unit of V/$\sqrt{\text{Hz}}$ generated in the absence of a signal. In order to obtain the TMR sensor limit of detection (LoD) in unit of T/$\sqrt{\text{Hz}}$, the following equation is used:

$$\text{LoD}(\text{T}/\sqrt{\text{Hz}}) = \frac{\text{LoD}(\text{V}/\sqrt{\text{Hz}})}{\text{Sens}(\text{mV/V/Oe}) \times \text{V}_{\text{bias}}(\text{V}) \times \text{Gain}(\text{V/V})} \quad (1)$$

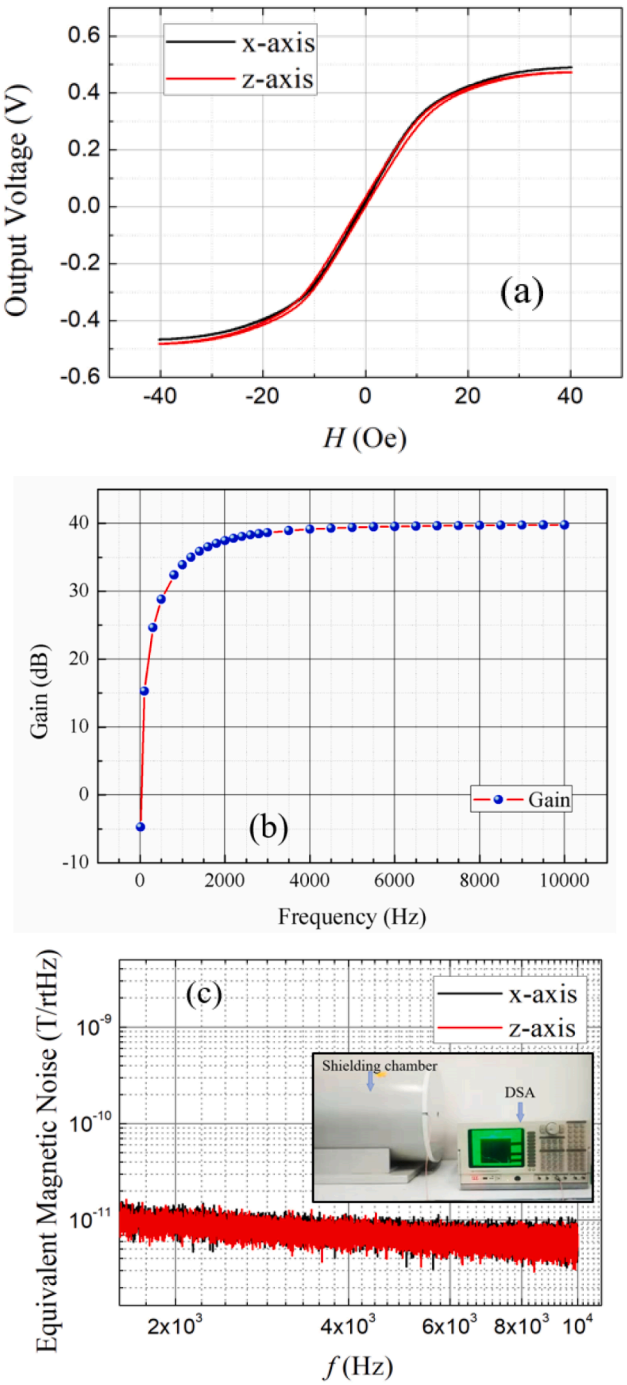

Fig. 1. (a) Sensitivity curves of the used TMR sensing elements; (b) Gain factor curve of the designed conditioning circuit; (c) LoD of TMR sensors, the inset is the noise detection system picture.

It is known that the excitation signal frequency of a typical ACFM system is invariably set at certain high frequency confined to the thermal noise range of the employed magnetic sensor. Fig. 1 (c) reveals that the TMR sensor exhibits rather flat thermal noise floor in frequency range of 1.6 to 10 kHz. It should be noted that the excitation signal frequency in this ACFM system is set at 3 kHz. From Fig. 1 (c), the LoD is measured to be around 9pT/$\sqrt{\text{Hz}}$ at $f = 3$ kHz. Compared with previous reported TMR based ACFM system, the extreme low magnetic noise that we observed using TMR composites coupled with a conditioning circuit represents an excellent pico-Tesla level LoD [30]. The extreme low noise and high sensitivity of such TMR sensor make it particularly promising

for use in ACFM applications for week magnetic field detection settings, for example small defect, high lift-off distance and sub-surface fatigue sensing. Under a demanding condition of lift-off = 10 mm, the detectability of this ACFM-TMR system is verified in Section 4.

2.2. Detection setup

The ACFM testing system is developed as shown in Fig. 2 (a). Such TMR sensor is used to measure the B_x and B_z magnetic field under a probe comprised of a nonferric yoke and a coaxial excitation coil of 250 turns. A functional generator (AFG1022, Tektronix, USA) provides a sine waveform signal for the excitation coil at frequency of $f = 3$ kHz and magnitude of $V_{pp} = 2$ V. The probe driven by a *DC* power supplier with the $V_{bias} = 2.5$ V (E36311A, Keysight, USA) can move above a workpiece with a lift-off distance of 1 mm, where there is an artificial longitudinal crack of 0.6 mm wide, 39 mm long and 6 mm deep. The workpiece is a square carbon steel (Q235B), which is widely used in the ship and bridge building. A datalogger (USB-6210, National Instruments, USA) is employed to receive the output analogue signal from the sensor. The photo of the ACFM testing system is shown in Fig. 2 (b).

3. Wavelet denoising

In this section, the denoising effect of proposed *TO* method with respect to other metrics is studied. Initially, the wavelet selection principle is introduced in section 3.1. Then, the selection of optimum mother wavelet and *DL* by *TO* method is indicated in section 3.2, whose performances are compared with other selection metrics in section 3.3.

3.1. Wavelet selection principle

Fig. 3 (a) and (b) show the collected B_x and B_z ACFM signal, respectively. It should be noted that the raw signal is significantly overlapped with the noise interferences that arise from the lift-off variations, mechanical vibration, porosity of specimen and electronic noise. Particularly, the critical points normally used to interpret the crack physical dimensions are hardly to be identified. Such noisy signal makes it difficult for researchers to predict the crack size accurately.

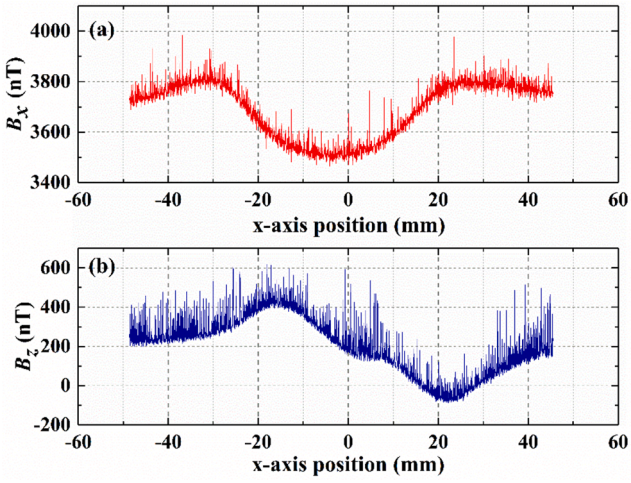

Fig. 3. The original (a) x-axis and (b) z-axis ACFM signal.

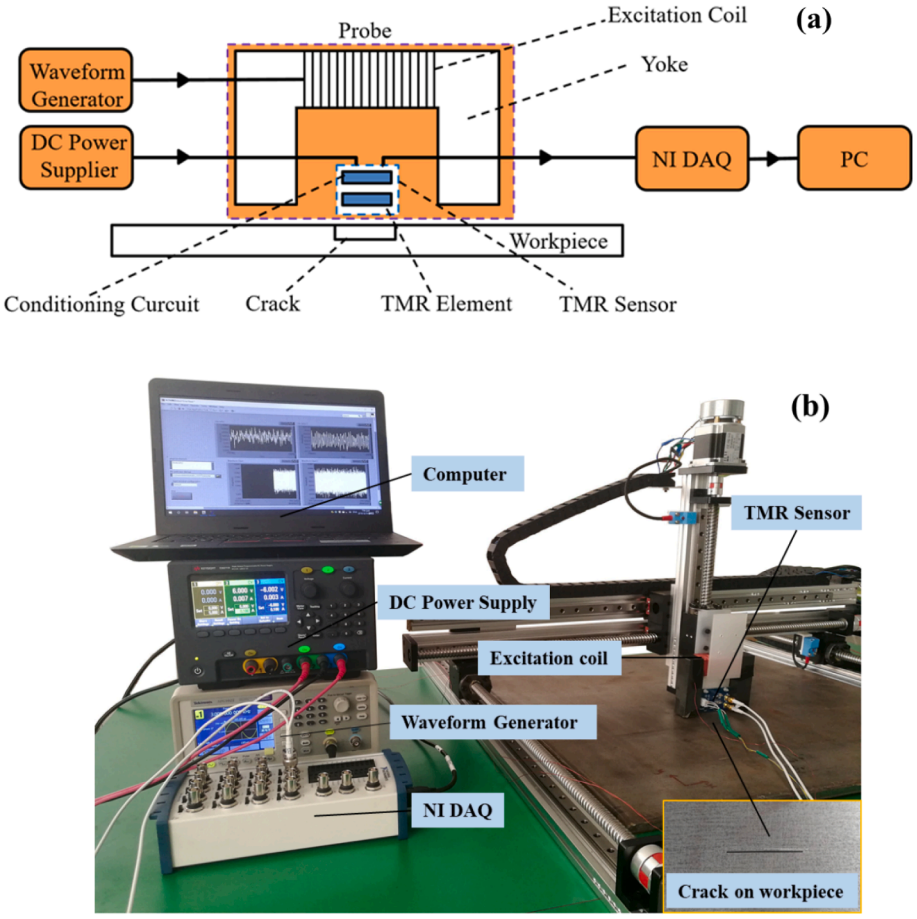

Fig. 2. (a) Detection system configuration picture; and (b) Photo of experimental system. The inset shows a crack sample on the workpiece.

3.1.1. Property matching

Selection of the optimal wavelet base is an annoying technical challenge in ACFM signal denoising. To start with, a pre-selection procedure of property matching allows substantial advance in solving the problem. There are seven fundamental base properties, which are orthogonality, compact support, symmetry, *CWT* (continuous wavelet transforms), *DWT* (discrete wavelet transforms), vanishing moment and regularity. Table 1 summarizes the seven base properties and eight popular wavelet families, which are Morlet, Mexican hat, Meyer, BiorNr-Nd, Haar, Daubechies, Symlets and Coiflets [31]. Selection of qualified base properties for ACFM signal denoising is established as follows.

(a) In wavelet transform applications, long-time signal collection and large amount of data process produce heavy computation burden, making *DWT* desirable for ACFM signal denoising. The *CWT* of a signal *f*(t) should be defined as following [31]:

$$CWT(a,\tau)=\frac{1}{\sqrt{a}}\int_{-\infty}^{\infty}f(t)*\varphi^{*}\left(\frac{t-\tau}{a}\right)dt \tag{2}$$

where φ^* is the conjugate of the wavelet base φ, α and τ are the continuous scale and translation factors, which increase gradually with a small calculating step and further incur considerable computation workload. In comparison, DWT is defined by:

$$DWT(j,k)=\frac{1}{\sqrt{a_0^j}}\int_{-\infty}^{\infty}f(t)*\varphi_{j,k}^{*}\left(\frac{t-ka_0^j\tau_0}{a_0^j}\right)\quad j\in Z,k\in Z \tag{3}$$

wherein, the discrete factors of α_0 and τ_0 are always set at 2 and 1, respectively. The comparison of the equation (2) and (3) shows that the discrete binary scale factor α and translation factor τ are employed by *DWT* to reduce the amount of the calculation.

(b) As the ACFM signal is a transient response to a minute crack, the abrupt information could be provided in a short time. Thus, the property of compact support should be chosen. This property enables the wavelet base to have good local property and rich short-term signal characteristics in time domain, and reduce signal computation burden equally.

(c) Because the high signal energy concentration is found to be beneficial for the signal data compression and denoising. The base property of regularity is required to reconstruct the signal image with smooth details, which is related with the energy concentration of the signal in frequency domain.

(d) Theoretically, the wavelet base with certain vanishing moment is desirable, which helps to clarify the signal approximation information, and reconstruct the original signal waveform. Meanwhile, the time and amplitude information of signal saltation points can be obtained accurately.

(e) The ACFM signal denoising is in favor of the property of orthogonality, which contributes to the precise reconstruction of the denoised signal.

(f) When the ACFM signal is decomposed or reconstructed, the property of symmetry is indispensable to minimize the signal distortion.

As discussed above, the necessary base properties are *DWT*, compact support, symmetry, regularity, orthogonality and certain vanishing moment. According to Table 1, the qualified wavelet bases are found to be Haar, Daubechies, Symlets and Coiflets. It should be noted that Haar is the same as *Db1* when the order *N* is set to one. To this end, twenty-one qualified mother wavelets are pre-selected, which are *SymN* (*N* from 1 to 8), *CoifN* (*N* from 1 to 5) and *DbN* (*N* from 1 to 8).

3.1.2. TO evaluation method

In this survey, the *TO* method is applied in assessment to select the optimal combination of mother wavelet and *DL* in a comprehensive sense. It is based on the analysis of the four-evaluating metrics of *CC, SNR, MSE* and *F*. The definitions and equations of these metrics are as follows [32]:

(a) *CC* represents the similarity between the theoretical and denoised signal waveforms, which can be computed by the following equation:

$$CC=\frac{cov(f',f^{*})}{\sqrt{var(f')var(f^{*})}} \tag{4}$$

where $cov(f',f^*)$ is the covariance between the denoised signal f' and the simulated signal f^*; $var(f')$ and $var(f^*)$ represent the variance of signal f' and f^*, respectively.

(b) *SNR* reflects the proportional relation between the useful signal power to that of the noise. Following is the function of *SNR*:

$$SNR=10log_{10}\left(p_S/p_N\right) \tag{5}$$

where p_S and p_N are the signal power and noise power, respectively.

(c) *MSE* describes the overall error of the signal after denoising, which provides another degree of freedom to compare the original signal with the denoised signal. *MSE* is expressed as follows:

$$MSE=\frac{\sum_{i=1}^{n}(f(i)-f'(i))^2}{n} \tag{6}$$

where f and f' represent the original and denoised signal, respectively; n represents the total amount of the signal.

(d) *F* can reflect the local variability of the signal, which is the unique criterion concentrating on the low-frequency approximation information of the signal. The coefficient *F* is defined as follows:

$$F=\frac{\sum_{i=1}^{n}[f'(i+1)-f'(i)]^2}{\sum_{i=1}^{n}[f(i+1)-f(i)]^2} \tag{7}$$

In a word, *CC, SNR* and *MSE* have the merit in evaluating the overall

Table 1
The properties of available popular wavelet bases.

Wavelet Base Property	Morlet	Mexican hat	Meyer	BiorNr-Nd	Haar (Db1)	Db (N)	Symlets (N)	Coiflets (N)
orthogonality	No	No	Yes	No	Yes	Yes	Yes	Yes
compact support	No	No	No	Yes	Yes	Yes	Yes	Yes
symmetry	Yes	Yes	Yes	Approx.	Yes	Approx.	Approx.	Approx.
CWT	Yes	Yes	Yes	Yes	Yes	Yes	Yes	Yes
DWT	No	No	Yes	Yes	Yes	Yes	Yes	Yes
vanishing moment	–	–	–	Nr-1	1	N	N	2 N
regularity	No	No	Yes	No	Yes	Yes	Yes	Yes

characteristics of the original signal while *F* specializes in assessing the detailed signal features and revealing the local bias of the signal.

The definition of *TO* is as follows [33]:

$$TO = \frac{(SNR_j)(CC_j)}{(F_j)(MSE_j)} j = 1 \ldots n \tag{8}$$

where CC_j, SNR_j, MSE_j and F_j denote the data sets of the four performance criteria of the denoised ACFM signal, *n* is the total amount of the combinations of various wavelet bases and decomposition levels. It is understood intuitively that large values of *SNR* and *CC* plus small values of *MSE* and *F* can result in better performance of denoising. Thus, according to equation (8), the maximum *TO* value refers to the best denoising effect, which introduces a comprehensive assessment strategy.

3.2. Selection of optimum combination of mother wavelet and DL

3.2.1. x-axis ACFM signal

Fig. 4 shows comparison of *TO* value diagrams of x-axis ACFM signal for three group mother wavelet families of (a) *SymN,* (b) *CoifN* and (c) *DbN* as a function of different *DLs*. Eight wavelet *SymN* (from 1 to 8) combine with seven *DLs* (from 3 to 9) to produce fifty-six combinations, as shown in Fig. 4 (a). Clearly, it can be seen that wavelet *Sym7* + *DL8* has the maximum *TO* value, which can be regarded as the best candidate in this wavelet family. Fig. 4 (b) illustrates that the largest *TO* value in *CoifN* family is related to *Coif5* + *DL8*. Among the fifty-six combinations of *DbN* family shown in Fig. 4 (c), *Db5* + *DL8* yields the highest *TO* value. The *TO* values of the three pre-selected combination in each wavelet family is presented in Table 2. The results suggest that wavelet *Db5* + *DL8* has the largest *TO* value of one unit among all wavelets, which can serve as the best candidate for x-axis ACFM signal denoising.

3.2.2. z-axis ACFM signal

Fig. 5 shows the *TO* results for z-axis ACFM signal with respect to the three interested mother wavelets. Fig. 5 (a), (b) and (c) show that wavelet *Sym7, Coif4, Db8* under *DL8* have the larger *TO* values than the others in every corresponding wavelet family, respectively. Table 3 indicates that *Sym7* + *DL8* has the highest *TO* value among such pre-selected three combinations, which can be identified as the optimal combination for z-direction ACFM signal denoising.

3.3. Denoising performance analysis

We summarize the x-axis detection performance of various combinations of mother wavelets (*SymN*, *CoifN* and *DbN*) and *DLs* with respect to four standard metrics (*SNR*, *F, CC* and *MSE*) and *TO* method. (Data is not shown here) It is found that the combination of *Sym7* + *DL8* refers to max(*CC*), the combination of *Db4* + *DL9* produces max(*SNR*), and the combination of *Db6* + *DL9* and *Db5* + *DL3* correspond to min(*F*) and min (*MSE*), respectively.

Table 2
Largest *TO* values in each wavelet family of *SymN, CoifN* and *DbN* for x-axis ACFM signal.

Wavelet base	Sym7	Coif5	Db5
DL	8	8	8
TO	0.98197	0.96393	1.00000

Fig. 6 (a) shows the x-axis denoised signal by applying the selected optimum combinations (*Db5* + *DL8*, see Table 2) based on *TO* method, which is compared with other four single evaluating criteria (maximum *CC*, maximum *SNR*, minimum *F* and minimum *MSE*). In Fig. 6 (a), it can be seen that employment of max(*SNR*) and min(*F*) metrics incur signal distortion, which is indicated by arrow 1 and 2, respectively. Also, the execution of min(*MSE*) inflicts insufficient noise depression, which is manifest by arrow 3. The signal denoising performed by max(*CC*) is close to that by max(*TO*), as the denoised signal curves are overlapped by each other. It is observed that performances of max(*TO*) and max(*CC*) are best in comparison to other criteria under test, allowing signal to be well reconstructed with minimal distortion.

The denoising performance for z-axis ACFM signal is also examined by the same five criteria as a function of different combinations. (Data is not illustrated here) It is found that the combinations of *Db6* + *DL8*, *Sym1* + *DL9*, *Db8* + *DL9* and *Db6* + *DL3* result in max(*CC*), max(*SNR*), min(*F*) and min(*MSE*) respectively, which can be regarded as the best candidates for each standard metric.

The denoising performance on z-axis ACFM signal is then analyzed by implementing the one having the largest *TO* value (*Sym7* + *DL8*, see Table 3) and the best candidates in each other evaluating criteria, as shown in Fig. 6 (b). It should be noted that the use of *Sym1* + *DL9* corresponding to max(*SNR*) suffers from serious signal distortion as marked by arrow 1, though low order of vanishing moment ($N = 1$) can introduce some smoothness. The denoised signal by *Db8* + *DL9* relate to min(*F*) tends to deviate from the original signal, where is labeled by arrow 2; whereas, *Db6* + *DL3* combination relate to min(*MSE*) renders incomplete noise elimination as highlighted by arrow 3. Again, max(*TO*) and max(*CC*) both yield the best denoising capability on z-axis ACFM signal. While the max(*CC*) has been observed to result in good denoising performance as the same as max(*TO*) in this case, we believe that the max(*TO*) is physically the best solution according to equation (4), and supportive of the experimental results shown in Section 3.1. The results provide a comparative study of advantage of *TO* method over the other evaluating rules used in denoising of the ACFM signal, as it considers four metrics simultaneously.

Further comparison between the proposed wavelet denoising method and the widely used LPF is done [34,35]. Fig. 7 illustrates the denoising performance by the wavelet denoising method and the LPF procedure with cut-off frequency f_c = 5, 10 and 20 Hz, respectively. Fig. 7 (a) and (b) indicate that the denoising capability of LPF declines with increasing f_c from 5 to 20 Hz. The LPF at f_c = 5 Hz presents smoothed curve, but it experiences some undesirable signal distortion.

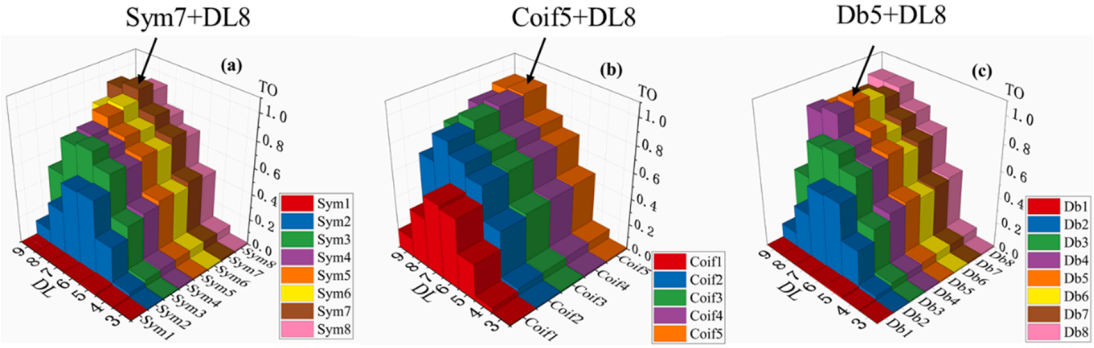

Fig. 4. *TO* value diagrams of x-axis ACFM signal by three mother wavelet families: (a) *SymN,* (b) *CoifN* and (c) *DbN* as a function of various *DLs*.

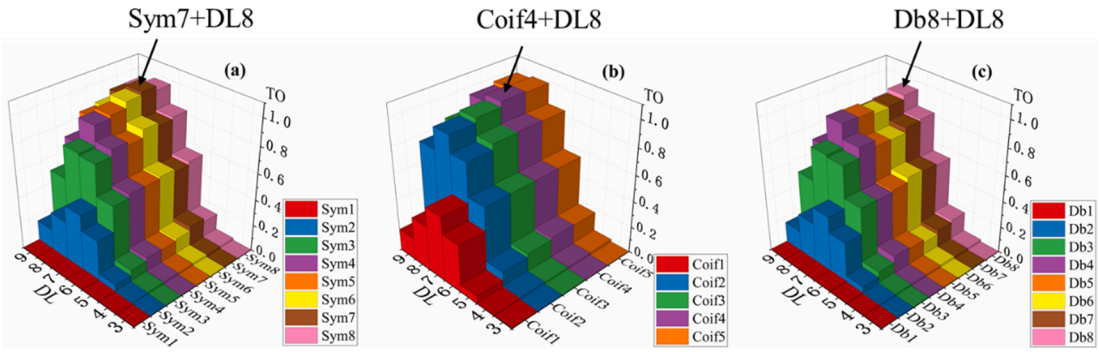

Fig. 5. *TO* value diagrams of z-axis ACFM signal by three mother wavelet families: (a) *SymN,* (b) *CoifN* and (c) *DbN* as a function of various *DLs*.

Table 3
Largest *TO* values in each wavelet family of *SymN, CoifN* and *DbN* for z-axis ACFM signal.

Wavelet base	Sym7	Coif4	Db8
DL	8	8	8
TO	1.00000	0.99762	0.94297

In comparison, the proposed wavelet denoising method provides a better signal reconstruction with little distortion than traditional LPF approach due to *TO* algorithm.

Theoretically, the crack's depth can be inversed by the measured B_x signal database [3]. Meanwhile, the two points with maximum and minimum strengths in B_z curve could be referred as the longitudinal beginning and end of the crack [36,37]. Thus the crack length can be

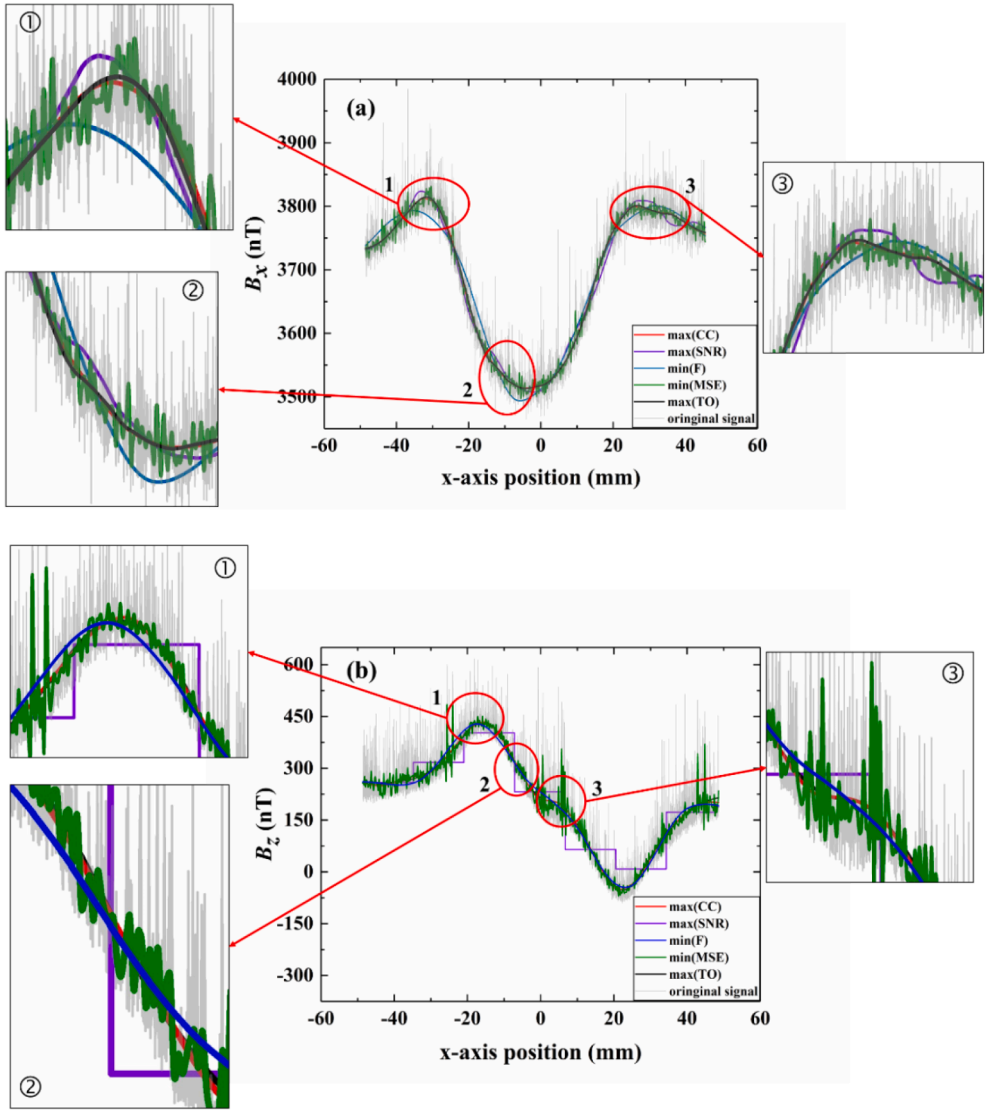

Fig. 6. Comparison of *TO* method with other four standard criteria for denoising performances in (a) x-axis ACFM signal B_x and (b) z-axis ACFM signal B_z.

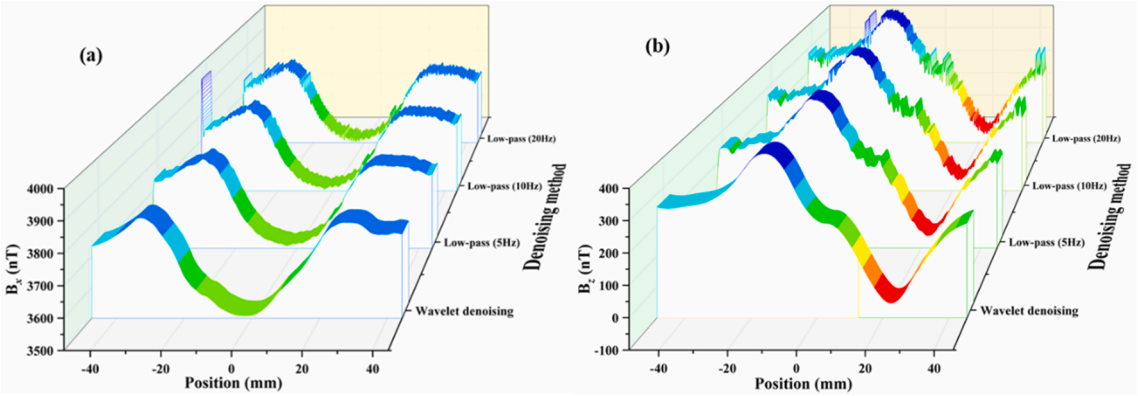

Fig. 7. (a) Denoised x-axis signal B_x by optimal wavelet denoising method and LPF; and (b) Denoised z-axis signal B_z by optimal wavelet denoising method and LPF.

estimated by measureing the distance between the two points along the x-axis.

The crack's depth is capable of being quantified according to the perturbed B_x strengths, which appear between the background baseline (line between points *A* and *B*) and the minimum strength (point *C*) position of the B_x curve, as illustrated in Fig. 8 (a). The background baseline is identified by points *A* and *B* referring to the defect-free area; while the minimum strength position in the B_x curve is labeled by point *C*. Points *A* and *B* located empirically are not representatives for the crack beginning and end points. In Fig. 8 (b), the clear peak point *D* and trough point *E* in the B_z curve could be employed to estimate the crack length as they can reflect the crack longitudinal beginning and end. The horizontal distance between points *D* and *E* is measured to be 38.5 mm, which is very close to the real crack length of 39 mm. The accurate crack sizing estimation arising from good denoising effect makes this ACFM detection system desirable for use in hard NDT application scenarios, such as tiny crack identification and harsh underwater operation conditions.

4. Verification experiment for improved system detectability

As discussed in Section 2 and 3, a block diagram of the proposed ACFM detection system is shown in Fig. 9 comprised of the TMR sensor probe and the *TO* algorithm. The TMR sensing elements which has high sensitivity and low self-noise are employed to obtain the induced magnetic field. A conditioning circuit is developed properly to amplify the sensing signal and suppress the unfavorable noise. Signal denoising is then carried out using *TO* algorithm to select the best-suited group of mother wavelet family and *DL*.

In order to examine the improved system detectability, a case study is then performed with demanding operation conditions. Keep all the

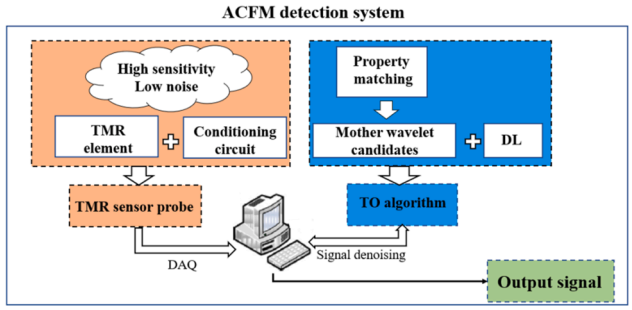

Fig. 9. Block diagram of proposed ACFM detection system comprised of TMR sensor probe and *TO* algorithm.

detection setup conditions the same as in Section 2.2, but increase the lift-off distance from 1 to 10 mm for the consideration of workpiece with thick protection layer or surface coating. As shown in Fig. 10 (a) and (b), one can see that it is hardly to extract useful information from the noisy original signal due to the decreased signal to noise ratio. The noise leaves ambiguity about the positions of the key points. As shown in Fig. 11, however, by applying the selected optimum combinations (*Db5* + *DL8* for x-axis signal, *Sym7* + *DL8* for z-axis signal) demonstrated in Section 3.2, the noise is significantly depressed. The key points of *A'*, *B'* and *C'* can be easily identified for x-axis signal in Fig. 11 (a), which can be used to estimate the crack's depth. Also, by pinpoint the critical points of *D'* and *E'* in Fig. 11 (b), the distance of *D'E'* is determined to be 38.3 cm which is a direct reflection of the crack length of 39 cm. According to equation (5), the original and denoised signal data shown in Fig. 11 could be employed to analyze the values. The *SNR* of the original

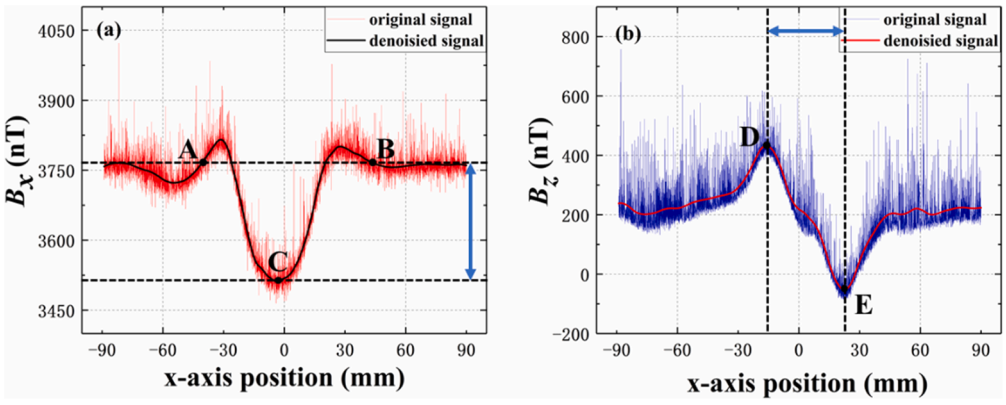

Fig. 8. (a) Denoised x-axis signal B_x by combination of *Db5* + *DL9*; and (b) Denoised z-axis signal B_z by combination of *Sym7* + *DL8*.

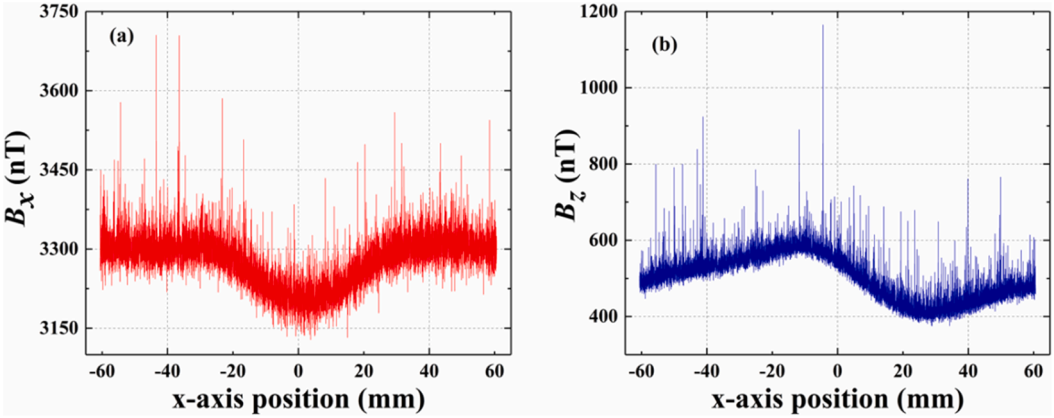

Fig. 10. The original (a) x-axis ACFM signal; and (b) z-axis ACFM signal with lift-off = 10 mm.

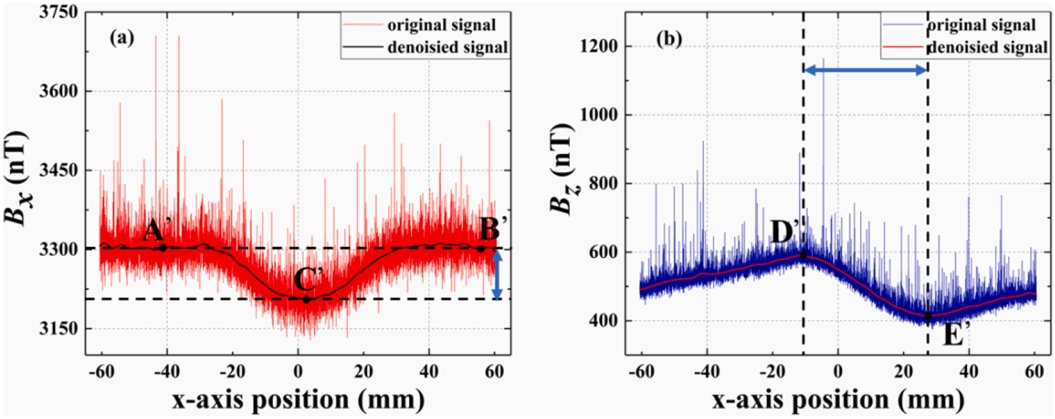

Fig. 11. (a) Denoised x-axis signal B_x by optimal combination of *Db5* + *DL8*; and (b) Denoised z-axis signal B_z by optimal combination of *Sym7* + *DL8*.

signal is given by the ratio of the power of the obtained raw signal part and the background noise part. The *SNR* of the denoised signal is defined by the ratio of the power of denoised raw signal part and background noise part. Upon that, an improved *SNR* of 25.5 dB is achieved for B_x signal as shown in Fig. 11 (a); while the *SNR* is enhanced by 16.5 dB for B_z signal as illustrated in Fig. 11 (b).

Clearly these experiment results demonstrate that the system detectability is favorably improved. The implementation of sensitive TMR sensor device and *TO* wavelet selection method add together to enhance the detection performance of this ACFM system. The achievement of such optimized ACFM system makes it capable to detect weak magnetic field with higher lift-off values. In particular, it is promising for this system to detect smaller target cracks without coating removal.

5. Conclusion

In this paper, a performance improvement scheme of a typical ACFM-TMR system is proposed in the sense of both hardware and software aspects. A novel double-axis TMR sensor is developed with high sensitivity of 30 mV/V/Oe in a detection range of ± 10 Oe and a LoD of 9pT/$\sqrt{}$Hz at $f \geq 3$ kHz. The sensing device is designed on condition of a gain transfer function of 100 × and a frequency bandwidth of larger than 1600 Hz. Such high-sensitive and low-noised TMR sensor is found to be adaptive for weak magnetic field detection in ACFM testing. Furthermore, our investigation provides direct evidence that the *TO* method can be employed to identify the optimal conditions of mother wavelet and *DL*. The selection principle is based on the comprehensive utilization of the four-standard metrics of *CC, SNR*, *MSE* and *F*. The results demonstrate the effectiveness of the scheme, and the combinations of *Db5* + *DL8* (see Table 2) and *Sym7* + *DL8* (see Table 3) are demonstrated as the most suitable combinations for the x- and z-axis ACFM signals denoising, respectively.

The *TO* selecting method has been recognized by previous studies for jet engine vibration signal denoising [33], but few quantitative analyses are available in ACFM application. Such merit in combination of advanced TMR device and effective denoising approach is important, which can be readily employed to predict the crack sizing under more pressing operation conditions of increased lift-off = 10 mm. The results yield that *SNR* is increased by 25.5 dB and 16.5 dB for x- and z-axis signal, respectively. The obtained ACFM-TMR system offers robust and less energy-consuming detection procedures that are vital for successful real-time NDT sensing. This give us a method attractive for real-time defects inspection of steel cable [17,18], and in-situ monitoring of composites manufacturing process [38,39].

Despite the consensus about the feasibility of ACFM schemes, there is significant room for system improvement. More robust and energy-friendly sensor device and sophisticated procedures for *SNR* improving, noise suppression, signal processing and interpretation remain confined to research field. One of the main problems is the lack of reliable transducer technology to pick up weak signal in condition of noisy environment and in-site processing. In particular, the workpiece with thick protection layer or coating also demands the large lift-off values and high accuracy for ACFM detection system. Indeed, implementation of ACFM schemes requires a pervasive approach of high detection capability, together with simple realization and low power consumption. Therefore, the employment of the low power TMR sensor and energy-saving *TO* denoising method is found to be very efficient for real world applications from a practical point of view, which is the first

step for the ACFM system optimization. It is intuitional and quantitative, so that it can be used to trigger a more profound inquiry for future works, which may include microcrack identification, large lift-off and compact system design.

Declaration of Competing Interest

The authors declare that they have no known competing financial interests or personal relationships that could have appeared to influence the work reported in this paper.

Acknowledgments

This work was supported in part by the Stable Supporting Fund of Acoustic Science and Technology Laboratory (JCKYS2020604SSJS006); the Natural Science Foundation of Heilongjiang Province of China (LH2019E040) and the Fund of Key Laboratory of Marine Intelligent Equipment and System Ministry of Education (MIES-2020-16).

References

[1] W. Li, G.M. Chen, W.Y. Li, Z. Li, F. Liu, Analysis of the inducing frequency of a U-shaped ACFM system, Ndt E Int. 44 (2011) 324–328.
[2] M.P. Papaelias, M.C. Lugg, C. Roberts, C.L. Davis, High-speed inspection of rails using ACFM techniques, NDT E Int. 42 (2009) 328–335.
[3] G.L. Nicholson, H. Rowshandel, X.J. Hao, C.L. Davis, Measurement and modelling of ACFM response to multiple RCF cracks in rail and wheels, Ironmak Steelmak 40 (2013) 87–91.
[4] W. Li, G.M. Chen, X.K. Yin, C.R. Zhang, T. Liu, Analysis of the lift-off effect of a U-shaped ACFM system, NDT E Int. 53 (2013) 31–35.
[5] G.L. Nicholson, A.G. Kostryzhev, X.J. Hao, C.L. Davis, Modelling and experimental measurements of idealised and light-moderate RCF cracks in rails using an ACFM sensor, Ndt E Int., 44 427-437.
[6] A. Akbari-Khezri, S.H.H. Sadeghi, Determination of Crack Depth Profile in Cylindrical Metallic Structures, Using Alternating Current Field Measurement Data, J. Nondestruct. Eval. 38 (2019) 8.
[7] A. Noroozi, R.P.R. Hasanzadeh, M. Ravan, A Fuzzy Learning Approach for Identification of Arbitrary Crack Profiles Using ACFM Technique, IEEE Trans. Magn. 49 (2013) 5016–5027.
[8] H. Rowshandel, G.L. Nicholson, J.L. Shen, C.L. Davis, Characterisation of clustered cracks using an ACFM sensor and application of an artificial neural network, NDT and E Int. 98 (2018) 80–88.
[9] S. Zhao, L. Sun, J. Gao, J. Wang, Y. Shen, Uniaxial ACFM Detection System for Metal Crack Size Estimation Using Magnetic Signature Waveform Analysis, Measurement 108090 (2020).
[10] M. Le, J. Kim, H.S. Do, J. Lee, 2-D Vector Field Visualization of Corrosion in a Small-bore Piping System using Bobbin-type Integrated Hall and GMR Sensors Arrays, 2014 IEEE Sensors Applications Symposium (SAS), Queenstown, New Zealand, 2014.
[11] Z. Li, R. Jarvis, P.B. Nagy, S. Dixon, P. Cawley, Experimental and simulation methods to study the Magnetic Tomography Method (MTM) for pipe defect detection, NDT E Int. 92 (2017) 59–66.
[12] C. Ye, Y. Huang, L. Udpa, S.S. Udpa, Novel Rotating Current Probe With GMR Array Sensors for Steam Generate Tube Inspection, IEEE Sens. J. 16 (2016) 8.
[13] T.J. Rocha, H.G. Ramos, A. Lopes Ribeiro, D.J. Pasadas, Magnetic sensors assessment in velocity induced eddy current testing, Sens. Actuators, A 228 (2015) 55–61.
[14] X.a. Yuan, W. Li, G. Chen, X. Yin, J. Ge, W. Jiang, J. Zhao, Bobbin Coil Probe With Sensor Arrays for Imaging and Evaluation of LongitudinalCracks Inside Aluminum Tubes, IEEE Sens. J. 18 (2018) 8.
[15] J. Ge, W. Li, G. Chen, X. Yin, J. Liu, Q. Kong, X. Yuan, Investigation of optimal time-domain feature for non-surface defect detection through a pulsed alternating current field measurement technique, Meas. Sci. Technol. 29 (2018), 015601.
[16] X.a. Yuan, W. Li, G. Chen, X. Yin, J. Ge, W. Yang, J. Liu, W. Ma, Inner circumferential current field testing system with TMR sensor arrays for inner-wall cracks inspection in aluminum tubes, Measurement 122 (2018) 232–239.
[17] B. Wu, Y.J. Wang, X.C. Liu, C.F. He, A novel TMR-based MFL sensor for steel wire rope inspection using the orthogonal test method, Smart Mater. Struct. 24 (2015), 075007.
[18] X. Liu, J. Xiao, B. Wu, C. He, A novel sensor to measure the biased pulse magnetic response in steel stay cable for the detection of surface and internal flaws, Sens. Actuators, A 269 (2018) 218–226.
[19] Y.M. Lee, J. Hayakawa, S. Ikeda, F. Matsukura, H. Ohno, Effect of electrode composition on the tunnel magnetoresistance of pseudo-spin-valve magnetic tunnel junction with a MgO tunnel barrier, Appl. Phys. Lett. 90 (2007), 212507.
[20] S. Ikeda, J. Hayakawa, Y. Ashizawa, Y.M. Lee, K. Miura, H. Hasegawa, M. Tsunoda, F. Matsukura, H. Ohno, Tunnel magnetoresistance of 604% at 300K by suppression of Ta diffusion in CoFeB/MgO/CoFeB pseudo-spin-valves annealed at high temperature, Appl. Phys. Lett. 93 (2008), 082508.
[21] J. Hayakawa, S. Ikeda, Y.M. Lee, F. Matsukura, H. Ohno, Effect of high annealing temperature on giant tunnel magnetoresistance ratio of CoFeB/MgO/CoFeB magnetic tunnel junctions, Appl. Phys. Lett. 89 (2006), 232510.
[22] D. Katoozian, R.P.R. Hasanzadeh, A Fuzzy Error Characterization Approach for Crack Depth Profile Estimation in Metallic Structures Through ACFM Data, IEEE Trans. Magn. 53 (2017) 1–10.
[23] S.M. Ahmadkhah, R.P.R. Hasanzadeh, M. Papaelias, Arbitrary Crack Depth Profiling Through ACFM Data Using Type-2 Fuzzy Logic and PSO Algorithm, IEEE Trans. Magn. 55 (2019) 1–10.
[24] X. Qiu, W. Chao, X. Cui, J. Wei, Real-time pre-processing of the pulsed eddy current signal from continuous casting slabs, Insight 55 (2013) 136–141.
[25] B. Sasi, B.P.C. Rao, T. Jayakumar, B. Raj, Wavelet Transform-Based Denoising Method for Processing Eddy Current Signals, Res. Nondestr. Eval. 21 (2010) 157–170.
[26] Y. Zhang, W.F. Ding, Z.F. Pan, J. Qin, Improved Wavelet Threshold for Image Denoising, Front. Neurosci. 13 (2019) 7.
[27] M. Afzal, S. Udpa, Advanced signal processing of magnetic flux leakage data obtained from seamless gas pipeline, NDT and E Int. 35 (2002) 449–457.
[28] Z.H. Du, S.H. Liu, L. Wang, Selection of the optimal wavelet bases for wavelet denoising of partial discharge signal, International Conference on Signal Processing System, 2010.
[29] C.F. Cunha, A. Carvalho, M.R. Petraglia, A.C.S. Lima, An improved scale dependent wavelet selection for data denoising of partial discharge measurement, 2013.
[30] Xin'an, Yuan, Wei, Li, Xiaokang, Yin, Guoming, Chen, Jiuhao, Ge, In-service detection of longitudinal cracks on drill pipes using induced circumferential current.
[31] Y. Wang, S.J. Chen, S.J. Liu, H.X. Hu, Best wavelet basis for wavelet transforms in acoustic emission signals of concrete damage process, Russ. J. Nondestr. Test. 52 (2016) 125–133.
[32] S.M. Kay, Fundamentals of Statistical Signal Processing, Technometrics 37 (1993) 465–466.
[33] M.S. Sadooghi, S. Esmaeilzadeh Khadem, A new performance evaluation scheme for jet engine vibration signal denoising, Mech. Syst. Sig. Process. 76–77 (2016) 201–212.
[34] X.A. Yuan, W. Li, G.M. Chen, X.K. Yin, W.C. Yang, J.H. Ge, Two-Step Interpolation Algorithm for Measurement of Longitudinal Cracks on Pipe Strings Using Circumferential Current Field Testing System, IEEE Trans. Ind. Inform. 14 (2018) 394–402.
[35] L.C. Zhou, S.K. Ren, J. Zhou, I. Destech Publicat, The Design of ACFM Detective System's Driving Source Based on AD9959, Destech Publications Inc, Lancaster, 2015.
[36] Z. Wenpei, L. Zhang, Y. Su, T. Fang, Numerical simulation of a U-Shaped ACFM inducer, 2015.
[37] W. Li, X.A. Yuan, G.M. Chen, X.K. Yin, J.H. Ge, A feed-through ACFM probe with sensor array for pipe string cracks inspection, NDT E Int. 67 (2014) 17–23.
[38] A. Sirikham, Y. Zhao, H.Y. Nezhad, W. Du, R. Roy, Estimation of Damage Thickness in Fiber-Reinforced Composites using Pulsed Thermography, IEEE Trans. Ind. Inf. 15 (2019) 445–453.
[39] Y. He, R. Yang, X. Wu, S. Huang, Dynamic Scanning Electromagnetic Infrared Thermographic Analysis Based on Blind Source Separation for Industrial Metallic Damage Evaluation, IEEE Trans. Ind. Inf. 14 (2018) 5610–5619.